Progress In Electromagnetics Research B, Vol. 53, 187–203, 2013

EFFICIENT STRIP-MODE SAR RAW DATA SIMULATOR OF EXTENDED SCENES INCLUDED MOVING TARGETS

Liang Yang[1, 2, *], Wei-Dong Yu[1], Yun-Hua Luo[1, 2], and Shi-Chao Zheng[1, 2]

[1]Institute of Electronics, Chinese Academy of Sciences, Beijing 100190, China

[2]University of the Chinese Academy of Sciences, Beijing 100039, China

Abstract—An accurate and efficient SAR raw data generator is of considerable value for testing system parameters and the imaging algorithms. However, most of the existing simulators concentrate on the raw signal simulation of the static extended scenes and targets. Actually the raw signal simulator of the moving targets is highly desired to quantitatively support the application of the ground moving targets indication. The raw data simulation can be exactly realized in the time domain but not efficient especially when simulating an extended scene. As for the issues, the analytical expression for the 2-D signal spectrum of moving targets with constant acceleration is derived and a fast raw data simulation method in the 2-D frequency domain based on inverse ω-κ algorithm is proposed in this paper, where the inverse STOLT interpolation is applied to simulate the range-azimuth couple. So it is more efficient than the time domain one by making use of Fast Fourier Transform (FFT). Simulation results for a man-made scene and a real SAR scene are provided to demonstrate its validity and effectiveness.

1. INTRODUCTION

Synthetic aperture radar (SAR) is a powerful remote sensing technique, which can work in all weather conditions and day and night [1–6]. The ground moving targets indication (GMTI) is one of the most important applications for synthetic aperture radar [7–10], and the performance of the GMTI system can be analyzed and evaluated by modeling the

Received 2 May 2013, Accepted 9 July 2013, Scheduled 23 July 2013

* Corresponding author: Liang Yang (yangliang_mail@163.com).

whole system through simulation method. SAR raw data generator is essential for designing the new sensor, testing the imaging algorithm and devising inversion algorithm, so the raw data simulator is a hot issue in the research of SAR [11–21]. However, only static targets are taken into account in existing simulators while the moving targets are rarely discussed. So SAR raw signal generator of moving targets is required, particularly when the real raw data are not available yet.

The SAR raw signal simulation methods include time domain, the two-dimensional frequency domain, and the hybrid time/frequency domain. The time domain method can achieve a realistic simulation, but it is highly time consuming especially in the present of extended scenes. The two-dimensional frequency domain approach greatly reduces the computational load with respect to the time domain approach, and it can accommodate the space-varied range-azimuth coupling and senor trajectory deviations exactly. The hybrid time/frequency simulation is a trade-off of the above two methods. Nevertheless, few studies are reported on an efficient frequency domain raw signal simulation that includes not only fixed but also moving targets.

There are some SAR raw data generators (RDG) of moving targets with drawbacks and applied limits [22, 23]. Reference [24] simulates the raw data of moving point targets in the time domain; however, the efficiency cannot be tolerated in the present of distributed moving targets. In [25], the paper proposed an efficient SAR raw data generator of a scene that includes fixed and moving targets; nevertheless, it can only simulate the raw data of moving targets with constant speed. In addition, the precision of the simulator is not high enough because it uses the hyperbolic approximation during the derivation of the spectrum of the moving targets. As for above issues, this paper presents an accurate and efficient strip-mode SAR raw data simulator of extended scene included fixed and moving targets, where an general analytical slant range model is proposed and the corresponding point target reference spectrum (PTRS) is derived. The precision and efficiency of the method are analyzed in detail, and the simulator is verified through a mixed scene simulation experiment in the paper.

The paper is organized as follows. In Section 2, the point target reference spectrum of moving targets with constant acceleration is derived. In Section 3, the procedure of the proposed simulator is described in detail. In Section 4, the high performance of the proposed generator is verified by a mixed scene simulation experiment, where the accuracy verification and efficiency analysis is presented and discussed. Finally, in Section 5 some concluding remarks are reported.

2. GEOMETRY CONFIGURATION AND 2-D SIGNAL SPECTRUM

The geometry configuration for the strip-mode SAR including a moving target upon a fixed scene is shown in Fig. 1. In this figure, t is the slow time, O the start point, v the SAR platform velocity, and α the squint angle. A target denoted by $P(r_0, x_0)$ is located in the fixed scene with velocity v_r in the slant range direction and v_a in the azimuth direction. a_r and a_a are the target acceleration in the slant range and azimuth directions, respectively. The closest slant range from the platform to the point target $P(r_0, x_0)$ is r_0.

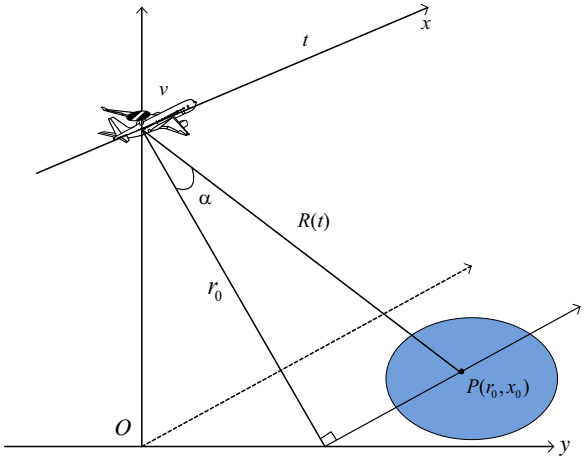

Figure 1. Strip-mode geometry.

According to the geometry in Fig. 1, the slant range between the platform and the target can be expressed as

$$R(t) = \sqrt{\left(r_0 - v_r t - \frac{1}{2}a_r t^2\right)^2 + \left(x_0 - (v - v_a)t - \frac{1}{2}a_a t^2\right)^2} \quad (1)$$

A 2-D signal spectrum is necessary in order to apply a fast raw data simulation method in the 2-D frequency domain. So the section derives the analytical spectrum of the moving target using the principle of stationary phase (POSP) [26].

Suppose that the received baseband signal from a point target is

$$G(s,t) = \sigma(r_0, x_0) \times \exp[-j4\pi f_0 R(t)/c] \times \exp\left[j\pi K_r (s - 2R(t)/c)^2\right] \quad (2)$$

where $\sigma(r_0, x_0)$ is the reflectivity coefficient of the point target; s and t represent the range and azimuth time variables respectively; c is the speed of light, f_0 the carrier frequency, and K_r the chirp rate.

Using the POSP and performing Fourier transformation (FT) with respect to range time, i.e.,

$$G(f_s,t)=\sigma(r_0,x_0)\times\exp\left(-j\pi f_s^2/K_r\right)\times\exp\left[-j4\pi(f_0+f_s)R(t)/c\right] \quad (3)$$

where f_s denotes the range frequency. To obtain the two-dimensional spectrum, a further Fourier transformation with respect to the azimuth time is performed. However, it can be observed that it is difficult to obtain the 2-D signal spectrum owing to the existence of the acceleration in the slant range (1). Instead a variable substituted and square method [27] is applied to reformulate the slant range history in order to circumvent the obstacle.

By Taylor expansion and discarding higher order terms induced by acceleration, the slant range (1) becomes,

$$\begin{aligned} R(t) &\cong \sqrt{R_0^2-2\left[r_0v_r+x_0(v-v_a)\right]t+\left[v_r^2+(v-v_a)^2-r_0a_r-x_0a_a\right]t^2} \\ &= \sqrt{\begin{array}{l} R_0^2-2R_0\left[\dfrac{r_0}{R_0}v_r+\dfrac{x_0}{R_0}(v-v_a)\right]t \\ \quad+\left[v_r^2+(v-v_a)^2-R_0\dfrac{r_0}{R_0}a_r-R_0\dfrac{x_0}{R_0}a_a\right]t^2 \end{array}} \\ &= \sqrt{\begin{array}{l} R_0^2-2R_0\left[\cos\alpha v_r+\sin\alpha(v-v_a)\right]t \\ \quad+\left[v_r^2+(v-v_a)^2-R_0\cos\alpha a_r-R_0\sin\alpha a_a\right]t^2 \end{array}} \end{aligned} \quad (4)$$

Changing the slant range (4) into the square, the following can be obtained

$$\begin{aligned} R(t) &= \sqrt{R_0^2-2R_0Nt+Mt^2}=\sqrt{\left(\frac{R_0N}{\sqrt{M}}-\sqrt{M}t\right)^2+\left(R_0^2-\frac{R_0^2N^2}{M}\right)} \\ &= \sqrt{\left(R_0\cos\varphi\right)^2+\left(R_0\sin\varphi-v_{eq}t\right)^2} \end{aligned} \quad (5)$$

where

$$R_0 = \sqrt{r_0^2+x_0^2} \quad (6)$$

$$M = v_r^2+(v-v_a)^2-R_0a_r\cos\alpha-R_0a_a\sin\alpha \quad (7)$$

$$N = v_r\cos\alpha+(v-v_a)\sin\alpha \quad (8)$$

$$v_{eq} = \sqrt{M} \quad (9)$$

$$\sin\varphi = \frac{N}{\sqrt{M}} \quad (10)$$

$$\cos\varphi = \sqrt{1-\frac{N^2}{M}} \quad (11)$$

Based on the transformed slant range (5) the accurate 2-D spectrum of moving target is given as follows,

$$G(f_s, f_t) = \sigma(r_0, x_0) \exp\left(-j\frac{\pi f_s^2}{K_r}\right) \exp\left(-j2\pi f_t \frac{R_0 \sin\varphi}{v_{eq}}\right) \exp\left(-j\frac{4\pi R_0 \cos\varphi}{c}\sqrt{(f_0+f_s)^2 - \frac{c^2 f_t^2}{4v_{eq}^2}}\right) \quad (12)$$

When all the motion parameters of the moving targets are equal to zero, the (12) becomes,

$$G(f_s, f_t) = \sigma(r_0, x_0) \exp\left(-j\frac{\pi f_s^2}{K_r}\right) \exp\left(-j2\pi f_t \frac{R_0 \sin\alpha}{v}\right) \exp\left(-j\frac{4\pi R_0}{c}\sqrt{(f_0+f_s)^2 - \frac{c^2 f_t^2}{4v^2}}\right) \quad (13)$$

It can be seen that (13) is the same as the spectrum of the fixed targets [26], which proves the accuracy of the derived 2-D spectrum of the moving targets. Then some remarks concerning about the last two terms of (12) will be made in order to understand the characteristic of the moving targets sufficiently.

$$\exp\left(-j2\pi f_t \frac{R_0 \sin\varphi}{v_{eq}}\right):$$

This term will decide the azimuth position of the moving target in the final imaging. In fact it also denotes the azimuth displacement by the range velocity of the target.

$$\exp\left(-j\frac{4\pi R_0 \cos\varphi}{c}\sqrt{(f_0+f_s)^2 - \frac{c^2 f_t^2}{4v_{eq}^2}}\right):$$

This term contains azimuth modulation, range cell migration and the high-order range-azimuth couple. Thus the term would result in the smear of the moving targets because it is modulated by the speed of the target.

With the precise 2-D spectrum model of moving targets a raw data simulator is designed which can generate the raw data of the extended scenes included the moving and static targets. In the next section the simulator will be introduced in detail.

3. RAW DATA SIMULATION

The raw signal simulation procedure for the extended scenes included fixed and moving targets is shown in Fig. 2(a), and the basic steps of the simulator are illustrated in Fig. 2(b).

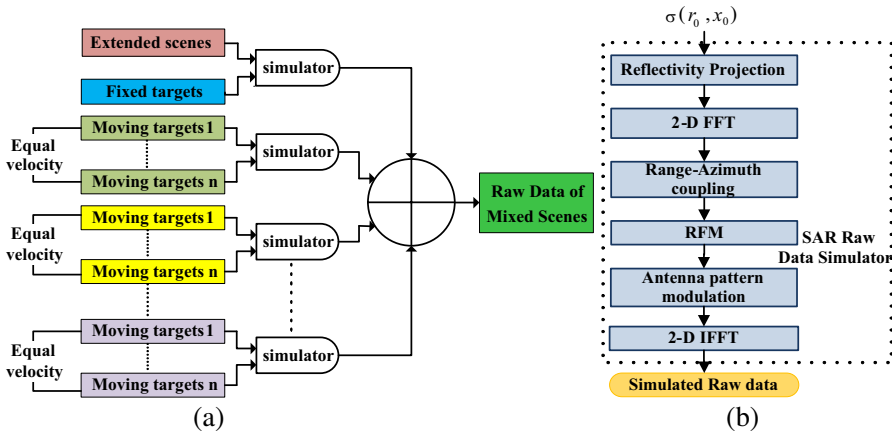

Figure 2. (a) Mixed scenes raw data simulation procedure. (b) Raw data simulator.

From Fig. 2(a), it can be seen that the proposed simulation method can generate raw data of mixed scenes which include extended scenes, fixed targets and moving targets with different velocities. First the simulator can generate the raw signal of the extended scenes and fixed targets at a time, where the fixed targets contain fixed point targets and fixed distributed targets composed of hundreds of point scatters. For the fixed targets, the targets velocities in the both directions can be set to be zero and then the simulator can generate the raw data very fast. Then the raw data of moving targets with different speed is generated, where the moving targets still include point targets and distributed targets. For the moving targets they should be classified with different velocities first of all, which may put the targets with the same motion parameters together and generate the raw signal at the same time with the simulator. It is important note that the moving distributed targets that composed of hundreds of moving point targets always have a threshold undivided size (TUS) such that the range velocities of the targets contained in can be assumed fixed, independent of the incidence angle [24]. When a big size moving distributed target exists, one may divide it in the range direction according to the threshold undivided size and then generate the raw data separately. Therefore, the raw data of the moving distributed targets can be simulated at a time and the consuming time is greatly reduced. After generating the raw signal of extended scenes, fixed targets and moving targets, they should be added together to get the strip SAR raw data of mixed scenes.

The simulator used in Fig. 2(a) is illustrated in Fig. 2(b). Based on

the signal spectrum model, the basic steps of the raw signal simulation are outlined as follows:

1) The reflectivity $\sigma(r_0, x_0)$ is projected to the imaging plane, the signal can be expressed as

$$g(s,t) = \iint G_r(s)\sigma(r_0, x_0)\delta(s - s_0)\delta(t - t_0)ds_0dt_0 \tag{14}$$

where $G_r(s)$ is the antenna beam pattern in the range directions, r_{ref} the reference slant range, and s_0 the propagation delay of the interested target corresponding to the one in the scene center, i.e.,

$$s_0 = \frac{2(R_0\cos\varphi - r_{ref})}{c} \tag{15}$$

2) 2-D Fast Fourier Transform (FFT) is performed to transform the signal into the 2-D frequency.

$$\begin{aligned} &G(f_s, f_t) \\ &= \iint G_r(s)\sigma(r_0, x_0)\exp[-j2\pi(f_0+f_\tau)s_0 - j2\pi f_t t_0]ds_0dt_0 \end{aligned} \tag{16}$$

3) The range frequency transition will be performed in the 2D frequency domain to simulate the range–azimuth coupling, i.e.,

$$\sqrt{(f_0 + f_s)^2 + \frac{c^2 f_t^2}{4v_{eq}^2}} \to f_s' \tag{17}$$

Inverse STOLT interpolation is applied to finish this step based on the above mapping relation. After the operation the signal becomes

$$G(f_s', f_t) = \iint G_r(s_0)\sigma(r_0, x_0)\exp\left[-j\Phi(f_s', f_t)\right]ds_0dt_0 \tag{18}$$

where

$$\Phi\left(f_s', f_t\right) = \frac{4\pi(R_0\cos\varphi - r_{ref})}{c}\sqrt{(f_0+f_s')^2 - \frac{c^2 f_t^2}{4v_{eq}^2}} + 2\pi f_t t_0 \tag{19}$$

4) Reference Function Multiplication (RFM) operation is applied to simulate all the range-invariant phase, thus the function is expressed as

$$\begin{aligned} H_{\mathrm{RFM}}(f_s', f_t) = &\exp\left\{-\frac{4\pi r_{ref}}{c}\sqrt{(f_0+f_s')^2 - \frac{c^2 f_t^2}{4v_{eq}^2}}\right\} \\ &\times\exp\left\{-\frac{2\pi f_t R_0\sin\varphi}{v_{eq}} + 2\pi f_t t_0\right\}\times\exp\left\{-\frac{\pi f_s'^2}{K_r}\right\} \end{aligned} \tag{20}$$

Then the simulation data becomes

$$G(f'_s, f_t) = \iint G_r(f'_s)\mathrm{rect}\left[\frac{f'_s}{B_r}\right] \times \sigma(r_0, x_0)\exp\left[-j\Phi\left(f'_s, f_t\right)\right] ds_0 dt_0 \quad (21)$$

where

$$\Phi(f'_s, f_t) = \frac{4\pi R_0 \cos\varphi}{c}\sqrt{(f_0+f'_s)^2 - \frac{c^2 f_t^2}{4v_{eq}^2}} + \frac{2\pi f_t R_0 \sin\varphi}{v_{eq}} + \frac{\pi f'^2_s}{K_r} \quad (22)$$

5) To make sure the generated raw data precise, the skewness of the spectrum in the frequency domain must be simulated. Thus the variance of the azimuth beam pattern $G_a(f_t)$ with the range frequency f_s should be taken into account. Neglecting the variation will result in the supporting area of the raw data deviate from the ideal area in the time domain. After the antenna pattern modulation, the signal is expressed as

$$G\left(f'_s, f_t\right) = \iint G_r\left(f'_s\right)\mathrm{rect}\left[\frac{f'_s}{B_r}\right] G_a(f_t) \times \sigma(r_0, x_0)\exp\left[-j\Phi\left(f'_s, f_t\right)\right] ds_0 dt_0 \quad (23)$$

6) Finally, after all the above operations, the raw signal is generated by applying 2-D Inverse Fast Fourier Transform (IFFT).

$$g(s,t) = \iint \sigma(r_0, x_0) G_r(s) G_a(t)\mathrm{rect}\left[\frac{s - 2R(t)/c}{T_r}\right] \times \exp[-j4\pi f_0 R(t)/c] \times \exp\left[j\pi K_r (s - 2R(t)/c)^2\right] ds_0 dt_0 \quad (24)$$

It can be seen the above simulation procedure bases on an inverse ω-κ algorithm, which can exactly simulate the high-order range-azimuth coupling. So it has high precision.

4. SIMULATION EXPERIMENT AND VALIDATION

4.1. Man-made Scenes Simulation

In this section, our work concentrates on the verification of the raw data of moving targets generated with proposed method. As we know, the most effective way to verify the precision of the generated raw data is to evaluate the corresponding imaging quality. The simulated raw data are validated based on the characteristic of the moving target imaging. The simulation system parameters are shown in Table 1. First, the raw data of a man-made scene are generated, which include fixed and moving point targets with different velocities, as presented in Fig. 3.

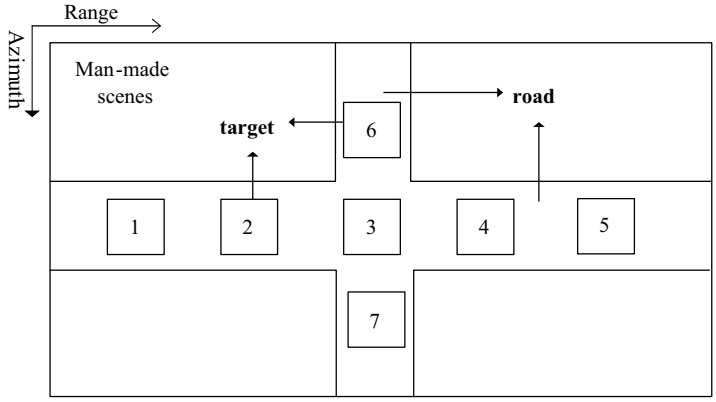

Figure 3. Man-made scene with fixed and moving targets.

Table 1. System parameters.

Parameters	Values
Carrier Frequency	9.6 GHz
Reference Range	10 km
Transmitted Bandwidth	150 MHz
Platform Velocity	150 m/s
Pulse Repeat Frequency	400 Hz
Pulse Length	2.5 μs
Antenna Azimuth Dimension	1 m
Squint Angle	0°/10°/30°

In this figure, the horizontal axis is the range direction, whereas the vertical is the azimuth direction. There are two roads parallel to the range and azimuth directions, respectively. There are seven targets of different velocities denoted by the rectangle with numbers, which are placed onto the road parallel to the range and azimuth directions, respectively. The velocities of targets are listed in Table 2. All of them are point targets in order to validate the raw data conveniently. As an expected backscattering phenomenon the reflectivity of the man-made scene is higher than the road.

The processed raw data are presented in Fig. 4, from which it can be seen that a focused image at the expected position is shown for the fixed target (T3); the targets (T1, T2) with range velocities show a azimuth shift phenomenon; the targets (T6, T7) with azimuth

Table 2. Motion parameters of moving targets.

Target No	1	2	3	4	5	6	7
$\mathbf{V_r}$ (m/s)	−1	0.5	0	0.5	−1	0	0
$\mathbf{V_a}$ (m/s)	0	0	0	1	1	2	5

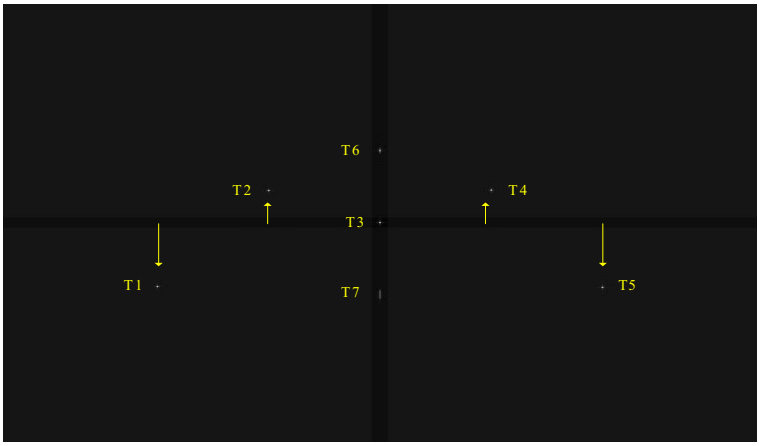

Figure 4. Focus result with raw data generated by the proposed simulator.

velocities represent the smear effect; the targets (T4, T5) with range and azimuth velocities show a displaced and smear phenomenon [28]. The above results prove the accuracy of the simulated raw data of the man-made scenes included fixed and moving targets initiatory. Then the raw data with proposed generator are validated specifically and verified by compare the two different simulation methods. The comparison result is shown in Table 3.

From Table 3, it can be observed that the azimuth shift induced by the range speed of moving target in frequency domain method agrees well with the time domain one in broadside mode (T1, T2), even in the presence of azimuth smear (T4, T5). In order to validate the raw signal sufficiently, the raw data of moving point target only with range velocities in squint mode are also simulated, and the result is given in Table 4, which also shows the error between frequency domain and time domain method is very tiny. For the moving targets with azimuth speed, the point target's smear width of 3-dB main lode is compared between the time domain method and the frequency domain method to validate the accuracy of the simulated raw data. As shown in Table 3, the azimuth smear widths based on our 2-D frequency method are

Table 3. Performance analysis of moving target based on different raw data simulation method.

Target No	Measured Frequency Domain values		Measured Time Domain Values	
	Azimuth Shift (m)	Azimuth Smear (m)	Azimuth Shift (m)	Azimuth Smear (m)
1	66.6660	0.9979	66.6700	0.9973
2	33.3350	0.9979	33.3400	0.9973
3	0	0.9981	0	0.9999
4	33.7800	1.0367	33.3300	1.0297
5	67.5650	1.0367	66.6650	1.0297
6	0	1.2539	0	1.2402
7	0	6.4800	0	6.1194

very close to that the time domain method, and the smear widths deteriorate with the increasing azimuth speed (T6, T7). In addition, the fixed target (T3) is well focused without any azimuth shift and azimuth smear. The above results prove the accuracy of the raw data of fixed and moving targets with proposed simulator.

In order to show the precision and effectiveness of the presented simulator, another simulation experiment is made to compare with the existing frequency domain generator introduced in [25]. The simulation parameters are the same as those in Table 1, and the compared result is given in Table 4.

Table 4. Performance analysis of moving target based on different raw data simulation method.

Azimuth shift(m)					
Vel(m/s)	**TDM**	**FDM-1**	**ERROR-1**	**FDM-2**	**ERROR-2**
Broadside mode					
$V_r = 0.5$, $V_a = 0$	33.3400	33.3276	0.0371%	33.3350	0.0149%
$V_r = 1.0$, $V_a = 0$	66.6700	66.6608	0.0137%	66.6660	0.0059%
Low squint mode					
$V_r = 0.5$, $V_a = 0$	33.3288	33.8250	1.4900%	33.3338	0.0150%
$V_r = 1.0$, $V_a = 0$	66.6652	67.8150	1.7200%	66.6675	0.0034%

In Table 4, the time domain method, the frequency method in [25], and the proposed method are labeled as TDM, FDM-1, and FDM-2, respectively. And ERROR-1 denotes the relative deviation between the TDM and FDM-1. ERROR-2 stands for the relative deviation between the TDM and FDM-2. The azimuth shift induced by the range velocities is the compared parameters since it can clearly reveal the accuracy of the three simulation methods. From Table 4, it can be seen that in the broadside mode, both of the frequency domain methods almost agree with the time domain one, where the relative error is at the acceptable level; however the proposed method exhibits a better performance. In the low squint mode (squint angle is 10°) it can be observed that the method in [25] shows a large relative deviation, which is not tolerable to the accuracy of the generated raw data. Nevertheless, the presented method still keeps a good performance, even in the case of high squint mode (squint angle is 30°), and the error is still within a small range by the simulation validation. Thus the proposed approach is more accurate than the other frequency domain simulator.

As we know, a tiny range acceleration will induce severe imaging unfocused, and it is difficult to apply quantitative method to analyze its accuracy. Thus the qualitative approach is applied to verify its effectiveness, and the result is shown in Fig. 5. It can be observed that the smear widths deteriorate with increasing acceleration, which proves the accuracy of the simulated data.

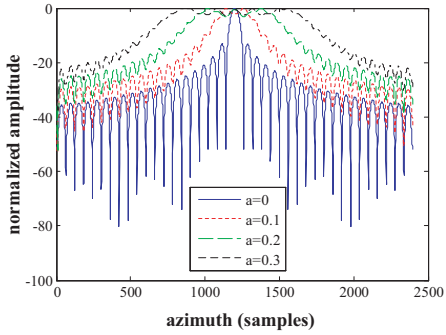

Figure 5. Azimuth smearing degree for different range acceleration.

4.2. Real SAR Scenes Simulation

In this section, a real scene simulation experiment is carried out to validate the proposed simulation method. The real SAR image is used as backscattering coefficients, as presented in Fig. 6(a). There are seven

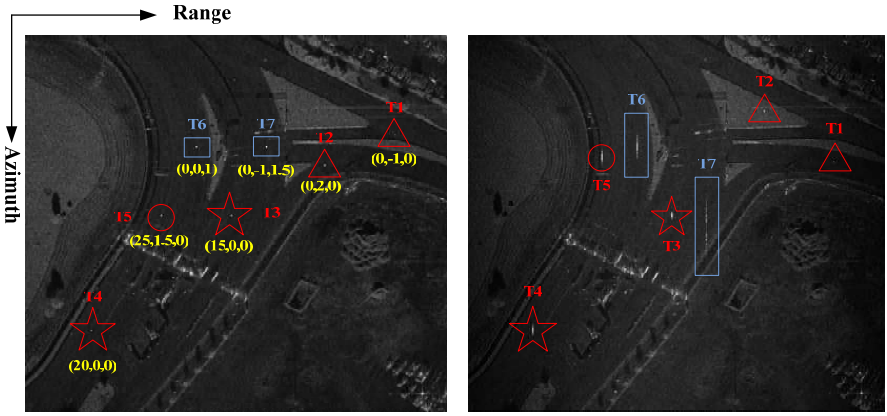

(a) (b)

Figure 6. (a) The simulation scene imaging with moving targets. (b) Focus result with raw data generated by the proposed simulator.

moving distributed targets which are artificially added with movement format of (v_a, v_r, a_r) as labeled in Fig. 6(a). The raw data of the mixed scene are simulated by the proposed method, and the processed raw data are presented in Fig. 6(b).

It can be observed that the focused result of the static scene is almost the same as the features of the real SAR image in Fig. 6(a), without any geometry deviation or defocusing. As for the moving targets in the scene, the targets (T1, T2) with only range velocities are displaced in the azimuth direction without the smear effect; the targets (T3, T4) with only azimuth velocities show an unfocused phenomenon, and the target (T5) with range and azimuth velocities generates above both effects; the targets (T6, T7) with range acceleration show a severe unfocused phenomenon; the target (T7) also shows a shift phenomenon owning to the range velocity. The above results prove the accuracy of the simulated raw data of the extended scenes included moving targets.

4.3. Efficiency Analysis

The primary advantage of the proposed raw data simulator is computational efficiency. The complex multiplication number is applied to compare the efficiency of the two simulation methods. And the computation of the proposed simulator with a single type of target can be expressed as

$$N_f = 10N_aN_r \log_2(N_aN_r) + 6N_aN_r + 2(2M_{\text{ker}} - 1)N_aN_r \qquad (25)$$

where M_{ker} is the length of interpolation kernel. N_a and N_r are the size of simulated scenes in the azimuth and range directions, respectively. The computation of the time domain simulator is

$$N_t = N_a^2 N_r^2 \tag{26}$$

It is difficult to estimate the efficiency of the proposed method directly owing to various kinds of targets. Instead supposing that in a simulated scene, there are $p\%$ targets belonging to moving point targets and $q\%$ is moving distributed targets with threshold undivided size (TUS) of K, and the remaining are fixed point targets and fixed distributed targets. So the accelerate ratio of the proposed method can be defined as

$$\eta = \frac{(N_a N_r * p\% + N_a N_r * q\%/K + 1)N_f}{N_t} \tag{27}$$

It can be observed that the efficiency of the proposed simulator mainly depends on the percentage of moving point targets and moving distributed targets. However, these targets usually take up very small portion of the whole simulated scene. Therefore, the mixed scene simulator can still demonstrate high efficiency. For example, a simulated scene contains 4096 bins in the range direction and 4096 bins in the azimuth direction, in which 0.001% belongs to moving point targets; 0.01% is moving distributed targets with TUS of $30 * 30$; the length of interpolation kernel is eight, then the accelerate ratio of this method is about 270 by calculation, which greatly reduces the simulation time with respect to the time domain method.

5. CONCLUSION

In this paper, a new strip-mode SAR raw data simulation approach of extended scenes included static and moving targets has been proposed. The proposed method can simulate the raw data of moving targets with constant acceleration and works well in the case of high squint comparing to the existing simulator. Meanwhile, it is more efficient than the time domain methods. The experiment results show its high performance for strip-mode SAR raw data simulation.

REFERENCES

1. Lim, S.-H., J.-H. Han, S.-Y. Kim, and N.-H. Myung, "Azimuth beam pattern synthesis for airborne SAR system optimization," *Progress In Electromagnetics Research*, Vol. 106, 295–309, 2010.

2. Liu, Q., W. Hong, W. X. Tan, Y. Lin, Y. Wang, and Y. Wu, "An improved polar format algorithm with performance analysis for geosynchronous circular SAR 2D imaging," *Progress InElectromagnetics Research*, Vol. 119, 155–170, 2011.
3. Wei, X., P. Huang, and Y.-K. Deng, "Multi-channel SPCMB-tops SAR for high-resolution wide-swath imaging," *Progress In Electromagnetics Research*, Vol. 116, 533–551, 2011.
4. Banasiak, R., R. Wajman, D. Sankowski, and M. Soleimani, "Three-dimensional nonlinear inversion of electrical capacitance-tomography data using a complete sensor model," *Progress In Electromagnetics Research*, Vol. 100, 219–234, 2010.
5. Park, J.-I. and K.-T. Kim, "A comparative study on ISAR imaging algorithms for radar target identification," *Progress In Electromagnetics Research*, Vol. 108, 155–175, 2010.
6. Wei, S. J., X. L. Zhang, and J. Shi, "Linear array SAR imaging via compressed sensing," *Progress In Electromagnetics Research*, Vol. 117, 299–319, 2011.
7. Zhou, W., J.-T. Wang, H. W. Chen, and X. Li, "Signal model and moving target detection based on MIMO synthetic aperture radar," *Progress In Electromagnetics Research*, Vol. 131, 311–329, 2012.
8. Tian, B., D.-Y. Zhu, and Z.-D. Zhu, "A novel moving target detection approach for dual-channel SAR system," *Progress In Electromagnetics Research*, Vol. 115, 191–206, 2011.
9. Sjogren, T. K., V. T. Vu, M. I. Pettersson, A. Gustavsson, and L. M. H. Ulander, "Moving target relative speed estimation and refocusing in synthetic aperture radar images," *IEEE Trans. on Aerosp. Electron. Syst.*, Vol. 48, No. 3, 2426–2436, 2012.
10. Lv, G. H., J. F. Wang, and X. Z. Liu, "Ground moving target indication in SAR images by symmetric defocusing," *IEEE Geosci. Remote Sens. Lett.*, Vol. 10, No. 2, 241–245, 2013.
11. Jin, Y.-Q., "Polarimetric scattering modeling and informationre-trieval of SAR remote sensing — A review of FDU work," *Progress In Electromagnetics Research*, Vol. 104, 333–384, 2010.
12. Buddendick, H. and T. F. Eibert, "Bistatic image formationfrom shooting and bouncing rays simulated current distributions," *Progress In Electromagnetics Research*, Vol. 119, 1–18, 2011.
13. Chang, Y.-L., C.-Y. Chiang, and K.-S. Chen, "SAR image simulation with application to target recognition," *Progress In Electromagnetics Research*, Vol. 119, 35–57, 2011.
14. Zhang, M., Y. W. Zhao, H. Chen, and W.-Q. Jiang, "SAR imaging

simulation for composite model of ship on dynamic ocean scene," *Progress In Electromagnetics Research*, Vol. 113, 395–412, 2011.

15. Alessandro, M. and D. V. Francesca, "A time-domain raw signal simulator for interferometric SAR," *IEEE Trans. on Geosci. Remote Sens.*, Vol. 42, No. 9, 1811–1817, 2004.
16. Franceschetti, G., M. Migliaccio, D. Riccio, and G. Schirinzi, "SARAS: A synthetic aperture radar (SAR) raw signal simulator," *IEEE Trans. on Geosci. Remote Sens.*, Vol. 30, No. 1, 110–123, 1992.
17. Wang, Y., Z. M. Zhang, and Y. K. Deng, "Squint spotlight SAR raw signal simulation in the frequency domain using optical principles," *IEEE Trans. on Geosci. Remote Sens.*, Vol. 46, No. 8, 2208–2215, 2008.
18. Qiu, X., D. Hu, L. Zhou, and C. Ding, "A bistatic SAR raw data simulator based on inverse ω-k algorithm," *IEEE Trans. on Geosci. Remote Sens.*, Vol. 48, No. 3, 1540–1547, 2010.
19. Franceschetti, G., R. Guida, A. Iodice, D. Riccio, and G. Ruello, "Efficient simulation of hybrid stripmap/spotlight SAR raw signals from extended scenes," *IEEE Trans. on Geosci. Remote Sens.*, Vol. 42, No. 11, 2385–2396, 2004.
20. Franceschetti, G., A. Iodice, S. Perna, and D. Riccio, "SAR sensor trajectory deviations: Fourier domain formulation and extended scene simulation of raw signal," *IEEE Trans. on Geosci. Remote Sens.*, Vol. 44, No. 9, 2323–2334, Sep. 2006.
21. Khwaja, A. S., L. Ferro-Famil, and E. Pottier, "Efficient SAR raw data generation for anisotropic urban scenes based on inverse processing," *IEEE Geosci. Remote Sens. Lett.*, Vol. 6, No. 4, 757–761, 2009.
22. Vachon, P. W., R. K. Raney, and W. J. Emery, "A simulation for spaceborne SAR imagery of a distributed, moving scene," *IEEE Trans. on Geosci Remote Sens.*, Vol. 27, No. 1, 67–78, 1989.
23. Franceschetti, G., V. Pascazio, and G. Schirinzi, "A SAR raw data simulator of nonstationary scenes," *Proc. Int. Geosci. Remote Sens. Symp.*, 2405–2408, 1990.
24. Rüegg, M., E. Meier, and D. Nüesch, "Constant motion, acceleration, vibration and rotation of objectsin SAR data," *Proc. of SPIE in SAR Image Analysis, Modeling and Techniques VII*, Vol. 5980, 598005, 2005, doi: 10.1117/12.626529.
25. Dogan, O. and M. Kartal, "Efficient strip-mode SAR raw-data simulation of fixed and moving targets," *IEEE Geosci. Remote Sens. Lett.*, Vol. 8, No. 5, 884–888, 2011.

26. Cumming, I. G. and F. H. Wong, *Digital Processing of Synthetic Aperture Radar Data Algorithms and Implementation*, Artech House, Norwood, MA, 2005.
27. Sun, B, Y. Zhou, J. Chen, and C. Li, "CA-ECS algorithm for squinted SAR imaging based on constant accleration model," *Acta Electron. Sin.*, Vol. 34, No. 9, 1595–1599, 2006.
28. Kersten, P. R., R. W. Jansen, K. Luc, and T. L. Ainsworth, "Motion analysis in SAR images of unfocused objects using time-frequency methods," *IEEE Geosci. Remote Sens. Lett.*, Vol. 4, No. 4, 527–531, 2007.